THE JOURNAL OF PHYSICAL CHEMISTRY B

ARTICLE

pubs.acs.org/JPCB

Electronic Quantum Fluxes during Pericyclic Reactions Exemplified for the Cope Rearrangement of Semibullvalene

Dirk Andrae,[†] Ingo Barth,[†,∥] Timm Bredtmann,[*,†] Hans-Christian Hege,[‡] Jörn Manz,[*,†] Falko Marquardt,[‡,§] and Beate Paulus[†]

[†]Institut für Chemie und Biochemie, Freie Universität Berlin, 14195 Berlin, Germany

[‡]Visualisierung und Datenanalyse, Zuse-Institut Berlin, 14195 Berlin, Germany

[§]Institut für Mathematik, Freie Universität Berlin, 14195 Berlin, Germany

ABSTRACT: The outcome of a pericyclic reaction is typically represented by arrows in the Lewis structure of the reactant, symbolizing the net electron transfer. Quantum simulations can be used to interpret these arrows in terms of electronic fluxes between neighboring bonds. The fluxes are decomposed into contributions from electrons in so-called pericyclic orbitals, which account for the mutation of the Lewis structure for the reactant into that for the product, in other valence and in core orbitals. Series of time-integrated fluxes of pericyclic electrons can be assigned to the arrows, for example 0.09−0.23 electrons for Cope rearrangement of semibullvalene, with hysteresis-type time evolutions for 27.3 fs. This means asynchronous electronic fluxes during synchronous rearrangement of all the nuclei. These predictions should become observable by emerging techniques of femto- to attosecond time-resolved spectroscopy.

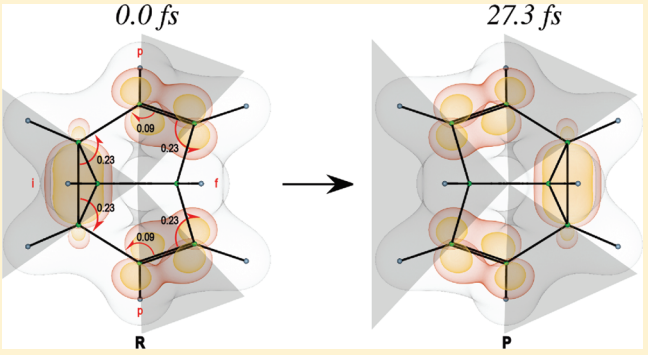

INTRODUCTION

Every chemist is familiar with the curved arrows in Lewis structures, symbolizing net electron transfer during pericyclic reactions. They represent the outcome of the reactions.[1] Many applications are documented in textbooks of organic,[2−6] inorganic,[7,8] and biochemistry.[9,10] In general, the tails and heads of the curved arrows indicate molecular bonds that are weakened and strengthened due to loss or gain of valence electron density during the reaction, respectively. Important examples include breaking bonds to the benefit of additional electrons in neighboring ones, or the formation of chemical bonds at the expense of electrons from neighboring ones. Previous theoretical investigations of pericyclic reactions have already focused on various aspects such as the Woodward−Hoffmann rules for the conservation of orbital symmetry,[11] analyses of transition structures or intermediates,[12−14] and assignments of concerted (or synchronous) versus sequential mechanisms.[15−17] Here we aim at quantum quantification of the arrows in Lewis structures. That means we shall determine the directions and the time evolutions of electronic fluxes, the numbers of electrons that are transferred, and the time of the pericyclic reaction in the electronic ground state, depending on the preparation of the reactants. For this purpose, we shall employ and extend our quantum dynamical approach for coupled electronic and nuclear fluxes in molecules in the electronic ground state,[18] which is based on fundamental developments in the quantum theory of fluxes by Miller and co-workers[19−22] (see also refs 23−25). This quantum approach is complementary to the theory of Takatsuka and co-workers, which is based on semiclassical Ehrenfest nuclear dynamics coupled to quantum electronic fluxes at sufficiently high energies allowing electronic transitions.[26−28] Our quantum results should stimulate experimental investigations of electronic fluxes during pericyclic reactions, by means of emerging concepts and techniques of femto- to attosecond chemistry.[29−36] In addition, we shall analyze the mechanisms. For this purpose, we shall decompose the net electronic fluxes and time-integrated fluxes (that is, the numbers of transferred electrons) into contributions of electrons in so-called pericyclic (k = peri), other valence (k = oval), and core (k = core) orbitals, respectively. Pericyclic orbitals are defined as the relevant subset of valence orbitals that describe the mutation of the Lewis structure of the reactant (R) to that of the product (P).

Scheme 1 shows three sets of curved arrows in the Lewis structure of R, for the degenerate 3,3-sigmatropic shift, or Cope rearrangement[37] of semibullvalene[38−62] (C_8H_8, SBV) in the electronic ground state. Also shown is the Lewis structure of P. R and P may be distinguished by partial deuteration. SBV may be considered as a derivative of the prototype compound 1,5-hexadiene, with a corresponding chain of six carbon atoms C6═C7−C8−C2−C3═C4 (R, clockwise notation, cf. Scheme 1), susceptible to the Cope

Special Issue: Shaul Mukamel Festschrift

Received: October 29, 2010
Published: January 25, 2011

Scheme 1. Lewis Structures of Semibullvalene (SBV) for Geometric Structures G = R and P of the Reactants and Products, with Pincer-Motion-Type, Counter-Clockwise, and Clockwise Curved Arrows, All Symbolizing the Same Outcome with Equivalent Net Electron Transfers

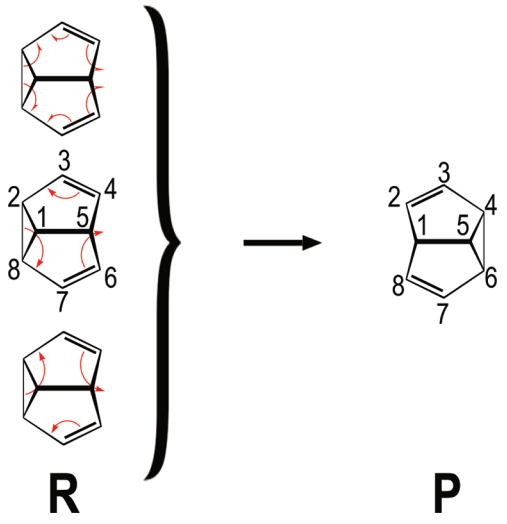

rearrangement to C2═C3−C4−C6−C7═C8 (P, keeping the labels of the carbon atoms), and a bridge of two carbon atoms C1, C5. This system and several derivatives have already served as touchstones for various properties that are related to pericyclic reactivity, from synthesis[38,42,50,51,58] via spectroscopy[39,41,49,53,56] and kinetics[39,40,48] to electronic structure[15,43,47,50−55,57−60] and the related thermochromicity,[45,50,51,53,58] ab initio molecular dynamics[61] and the role of tunneling,[62] and quantum dynamics simulations of laser control.[44−46] In fact, thermochromicity is supported by the low potential barrier between R and P, and by the large gap between the potential energy surfaces (PES) for the electronic ground and excited states.[44,53−55] That large energy gap also implies the validity of the Born−Oppenheimer approximation (BOA)[63−65] for the present quantum simulations of the Cope rearrangement of SBV in the electronic ground state—an important presupposition of our approach to coupled electronic and nuclear fluxes.[18]

The curved arrows in Scheme 1 are arranged in pincer-motion-type, counter-clockwise, and clockwise manners. All presentations correspond to the same outcome with equivalent net electron transfer, corresponding to breaking the C8−C2 bond (clockwise notation), formation of the C4−C6 bond, and double bond shifting from C3−C4 to C2−C3, as well as from C6−C7 to C7−C8. Our quantum quantification shall determine the specific set of curved arrows in the Lewis structure that symbolizes the bond-to-bond directions of electronic fluxes during Cope rearrangement of SBV, assign numbers of transferred electrons to each of the corresponding arrows, and evaluate the time evolutions of the electronic fluxes, together with the reaction time $t_r = t_P - t_R$ for the 3,3-sigmatropic shift from $t_R = 0$ fs for R to t_P for P, depending on the initial preparation of the reactant.

THEORY AND METHODS

Model. In order to quantify the bond-to-bond fluxes symbolized by the curved arrows in the Lewis structures, we consider the scenario where the Cope rearrangement of SBV proceeds on the PES V of the electronic ground state. The initialization of

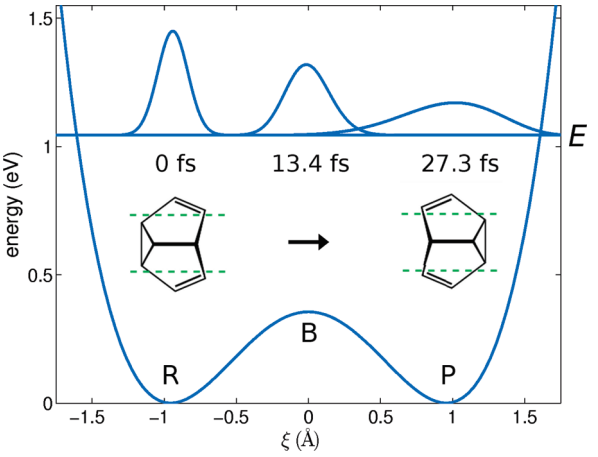

Figure 1. Cope rearrangement of SBV, from the reactant (R, $t_R = 0$ fs) via the potential barrier (B, $t = 13.4$ fs) to the product (P, $t_P = 27.3$ fs). Nuclear wavepacket dynamics from R via B to P are indicated by snapshots of the nuclear density, with baseline at the mean total energy E. Also shown is the underlying double well PES V versus the pericyclic coordinate ξ. Lewis structures for SBV in the configurations R and P are shown as an inset. Perpendicular observer planes for nuclear movement intersect at the green dashed lines.

pericyclic reactions in the electronic ground state has recently been demonstrated experimentally using an ultrashort laser pulse (5 fs).[66] For alternative approaches, see, e.g., refs 44, 67, and 68. In general, the details of the course of the reaction depend on the preparation of the reactants. We assume that the initial nuclear wave function, $\Psi_{nu}(\xi,t_R)$, is centered at the potential minimum for the reactants, $V_R = V(\xi_R)$, with momentum p_ξ along the path ξ to the potential minimum for the products $V_P = V(\xi_P)$. Our model simulation of the Cope rearrangement of SBV assumes sufficient initial kinetic energy such that the mean total energy E is above the potential barrier V_B (Figure 1). For this scenario, the time for the reaction, t_r, is so short (<30 fs, see below) that the motion along the coordinate ξ from ξ_R (<0) to ξ_P (= $-\xi_R$ > 0) is essentially decoupled from the other degrees of freedom, i.e., our quantum dynamics simulation of the pericyclic reaction of SBV will focus on wavepacket dynamics along the pericyclic coordinate ξ. This corresponds to synchronous nuclear motions, in accord with ab initio molecular dynamics simulations, even at elevated temperatures.[61] The decoupling is also supported by the structural constraints that are imposed on SBV (compared to the rather flexible large amplitude motions of 1,5-hexadiene) by the C1−C5 carbon−carbon bridge.[41]

The PES $V(\xi)$ along ξ is shown in Figure 1. It is evaluated by means of quantum chemical first-principles calculations based on Kohn−Sham density functional theory. The calculations are performed with the MOLPRO[69] program package, using the B3LYP functional[70,71] together with the cc-pVTZ[72] basis sets. The reliability of this method concerning structures and energies along the coordinate ξ is ensured by comparison to high-level ab initio methods (CASPT2/cc-pVTZ and MRCI/cc-pVTZ, CCSD(T)/cc-pVTZ, respectively). The corresponding one-particle electron density is denoted $\rho_{el}(\mathbf{r},\xi)$.

Nuclear Quantum Dynamics. The time evolution of the nuclear wave function on the PES $V(\xi)$ is evaluated as a solution of the time-dependent nuclear Schrödinger equation (TDNSE)

$$i\hbar \frac{\partial}{\partial t}\Psi_{nu}(\xi,t) = -\frac{\hbar^2}{2\mu}\frac{\partial^2}{\partial \xi^2}\Psi_{nu}(\xi,t) + V(\xi)\Psi_{nu}(\xi,t) \quad (1)$$

dx.doi.org/10.1021/jp110365g |J. Phys. Chem. B 2011, 115, 5476–5483

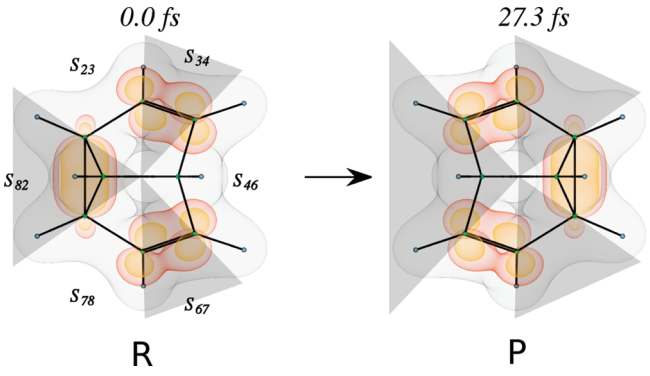

Figure 2. Bird's eye views of SBV for structures G = R and P, in a frame of Cartesian coordinates that are centered at the center of mass. The y-axis is parallel to the C8−C2 (clockwise notation, cf. Scheme 1) and C4−C6 bonds of R and P, respectively. The z-axis is perpendicular to the paper plane. Equidensity contours (values in units of a_0^{-3}; maximum values are given in brackets) illustrate the one-electron total density [gray: 0.047 (108)], and the partial density for electrons in pericyclic orbitals [red: 0.04, and yellow: 0.073 (0.42)]. Also illustrated are the sectors $S_{ij}(G)$ which are labeled according to the carbon−carbon bonds Ci-Cj of the chain of carbon atoms C6═C7−C8−C2−C3═C4 (clockwise notation) with the same labels for R and P. Each sector $S_{ij}(G)$ is bound by two half planes $A_i(G)$ and $A_j(G)$,which intersect at the z-axis and contain the nuclear centers of the neighboring carbon atoms Ci and Cj, respectively. The program Amira[74] was used for data visualization.

by means of the WavePacket[73] program on a set of 128 spatial grid points with step size $\Delta\xi$ = 0.0383 Å and time step Δt = 0.01 fs. The associated reduced mass is $\mu = (M_C + M_H)/4$[41] with nuclear masses M_C and M_H. The mean translational energy along ξ is set to $E_{trans} = \langle p_\xi^2/(2\mu)\rangle$ = 1.01 eV such that the mean total energy (E = 1.04 eV) is well below the first excited electronic state.[44,53−55] As a consequence, the reaction may be described quantum mechanically within the framework of the BOA.

Partitioning of the Electron Density. We partition the total electron density, $\rho_{el}(\mathbf{r},\xi)$, into contributions from eight core orbitals and 20 valence orbitals, $\rho_{el}(\mathbf{r},\xi) = \rho_{el,core}(\mathbf{r},\xi) + \rho_{el,val}(\mathbf{r},\xi)$. The latter are further partitioned by transformation into localized orbitals using the Pipek−Mezey[75] method. Three localized orbitals are identified as so-called pericyclic orbitals, i.e., those orbitals that correspond to the rearrangement of electrons according to the Lewis structures (cf. Scheme 1) and are illustrated as red and yellow equidensity contours in Figure 2. Thus, $\rho_{el}(\mathbf{r},\xi) = \rho_{el,core}(\mathbf{r},\xi) + \rho_{el,oval}(\mathbf{r},\xi) + \rho_{el,peri}(\mathbf{r},\xi)$ and the N = 56 electrons of SBV are partitioned into N_{peri} = 6, N_{oval} = 34, and N_{core} = 16 electrons occupying pericyclic, other valence, and core orbitals, respectively.

Electronic Fluxes. Following our method developed in ref 18, the mean electronic fluxes $F_{obs,k}(t)$ of pericyclic (k = peri), other valence (k = oval), core (k = core), or all (k = total) electrons out of or into a domain S_{obs} with volume $\mathcal{V}_{obs}$ through its surface A_{obs}, are calculated as

$$F_{obs,k} = \frac{d}{dt}\bar{N}_{obs,k}(t) = \frac{d}{dt}\bar{Y}_{obs,k}(t) \quad (2)$$

The subscript "obs" represents the definition of S_{obs} by the observer; in general, $S_{obs} = S_{obs}(\xi)$, $\mathcal{V}_{obs}=\mathcal{V}_{obs}(\xi)$, and $A_{obs}=A_{obs}(\xi)$ may depend on the nuclear configuration ξ, e.g., one may consider appropriate different domains for the reactants ($\xi = \xi_R$) and products ($\xi = \xi_P$) (see the application below).

The quantity $\bar{N}_{obs,k}(t)$ in eq 2 denotes the mean value of the number of electrons (k),

$$N_{obs,k}(\xi) = \int_{\mathcal{V}_{obs}(\xi)} d\mathbf{r}\rho_{el,k}(\mathbf{r},\xi) \quad (3)$$

in the volume $\mathcal{V}_{obs}(\xi)$ at time t,

$$\bar{N}_{obs,k}(t) = \int d\xi N_{obs,k}(\xi)\rho_{nu}(\xi,t) \quad (4)$$

where

$$\rho_{nu}(\xi,t) = |\Psi_{nu}(\xi,t)|^2 \quad (5)$$

denotes the nuclear density (c.f. eq 1). The difference

$$\bar{Y}_{obs,k}(t) = \bar{N}_{obs,k}(t) - \bar{N}_{obs,k}(t_R) \quad (6)$$

is the mean time-integrated flux of electrons (k) that have flown across the boundary A_{obs}, or, in other words, the accumulated number of electrons (k) that have been transferred accross the boundary A_{obs}, from t_R = 0 until time t. Positive or negative values of $\bar{Y}_{obs,k}(t)$ correspond to gains or losses of electrons (k) in the volume $\mathcal{V}_{obs}$, respectively. The letter "Y" represents the general term "yields" (= gains or losses).

Quantum effects are taken into account both via the electronic and the nuclear densities, $\rho_{el,k}(\mathbf{r},\xi)$ and $\rho_{nu}(\xi,t)$. In particular, $\rho_{nu}(\xi,t)$ displays nuclear dispersion. If one neglects those effects, one may consider just two ("classical") configurations ξ_R and ξ_P of the reactant R and the product P. Accordingly, the net time-integrated flux of electrons (k) from R to P is

$$Y_{obs,k} = N_{obs,k}(\xi_P) - N_{obs,k}(\xi_R) \quad (7)$$

This time-independent, classical limit may serve as a reference for the quantum time-integrated flux $\bar{Y}_{obs,k}(t = t_P)$, eq 6.

Monitoring Bond-to-Bond Electron Transfer. In order to quantify the bond-to-bond electronic fluxes during the pericyclic reaction, we introduce six sectors S_{ij}, specifically S_{23}, S_{34}, S_{46}, S_{67}, S_{78}, S_{82} (clockwise notation), with volumes $\mathcal{V}_{ij}(\xi)$ and surfaces $A_{ij}(\xi)$ (see Figure 2). Each surface $A_{ij}(\xi)$ consists of two half planes $A_i(\xi)$ and $A_j(\xi)$, which intersect at the z-axis and contain the nuclear centers of the neighboring carbon atoms Ci and Cj, respectively. Accordingly, the general expressions, eqs 2−4 and eq 6, are specified with the notations

$$F_{ij,k} = \frac{d}{dt}\bar{N}_{ij,k}(t) = \frac{d}{dt}\bar{Y}_{ij,k}(t) \quad (8)$$

$$N_{ij,k}(\xi) = \int_{\mathcal{V}_{ij(\xi)}} d\mathbf{r}\rho_{el,k}(\mathbf{r},\xi) \quad (9)$$

$$\bar{N}_{ij,k}(t) = \int d\xi N_{ij,k}(\xi)\rho_{nu}(\xi,t) \quad (10)$$

$$\bar{Y}_{ij,k}(t) = \bar{N}_{ij,k}(t) - \bar{N}_{ij,k}(t_R) \quad (11)$$

implying conservation of the numbers of electrons, $\bar{N}_k(t) = \sum_{S_{ij}}\bar{N}_{ij,k}(t) = \sum_{S_{ij}}N_{ij,k}(\xi) = N_k$. The net fluxes $F_{ij,k}(t)$ can be separated into two individual fluxes of electrons (k) through the surfaces A_i and A_j

$$F_{ij,k}(t) = F_{i,k}(t) - F_{j,k}(t) \quad (12)$$

The sign convention in eq 12 implies that clockwise fluxes $F_{i,k}(t)$ and $F_{j,k}(t)$ increase and decrease the number $\bar{N}_{ij,k}(t)$ of electrons

(k) in sector S_{ij}, respectively, and vice versa for anticlockwise fluxes.

The time-integrated fluxes

$$\overline{Y}_{j,k}(t) = \int_{t_R}^{t} d\tau F_{j,k}(\tau) \quad (13)$$

determine the numbers of electrons (k) that have flown from sector S_{ij} through the boundary A_j to sector S_{jl}, from time t_R until t. In analogy with eq 12,

$$\overline{Y}_{ij,k}(t) = \overline{Y}_{i,k}(t) - \overline{Y}_{j,k}(t) \quad (14)$$

The arrows in the Lewis structure pass from one sector, say S_{ij}, through the boundary A_j to the neighboring sector, say S_{jl}. Our quantification of the appropriate arrow in the Lewis structure is defined as the time-integrated flux of pericyclic electrons from sector S_{ij} to S_{jl} through the half plane A_j, during the reaction from $t = t_R$ to $t = t_P$, that is, the number $\overline{Y}_{j,\mathrm{peri}}(t_P)$ of pericyclic electrons that have been transferred from bond Ci−Cj to Cj−Cl, as defined in eq 13.

The numbers of pericyclic (k = peri), other valence (k = oval), and core (k = core) electrons $N_{ij,k}(\xi)$ in sectors $S_{ij}(\xi)$ are determined by quantum chemistry first-principles calculations of the partial one-electron densities on a fine spatial grid (150 × 150 × 150 points) by the same DFT method specified above, followed by numerical integrations in the sectors. The grids are centered at the center of mass and oriented parallel to the Cartesian coordinates. The step sizes are adapted such that for the individual sectors $S_{ij}(\xi)$, the nuclei of the carbon atoms Ci and Cj are centered in one of the cells of the grids. The total number of electrons in sector $S_{ij}(\xi)$ is

$$N_{ij,\mathrm{total}}(\xi) = N_{ij,\mathrm{core}}(\xi) + N_{ij,\mathrm{peri}}(\xi) + N_{ij,\mathrm{oval}}(\xi) \quad (15)$$

After evaluation of $N_{ij,k}(\xi)$, one solves the TDNSE (eq 1) and determines the time-integrated flux $\overline{Y}_{ij,k}(t)$ using eqs 8−11.

RESULTS AND DISCUSSION

At first we analyze the net electron transfer during the Cope rearrangement of SBV from reactant R to product P. Later on, the dynamics of this process is discussed, providing still deeper insight into the coupled electronic and nuclear quantum movement.

Time-Independent Analysis. As a first step, we select the appropriate set of arrows in the Lewis structure. The validity of the BOA implies that the electronic wave function of SBV in the nondegenerate electronic ground state is a real valued function. Exclusively clockwise or counter-clockwise electronic fluxes, however, carry electronic angular momentum, calling for complex valued functions.[76−78] Hence they are ruled out. In contrast, the pincer-motion type of electronic fluxes is appropriate, as symbolized in Scheme 1. It implies C_s symmetry during the pericyclic reaction. That means that the values of time-integrated electronic fluxes from sectors S_{82} to S_{23}, from S_{34} to S_{23}, and from S_{34} to S_{46} are the same as those from sectors S_{82} to S_{78}, from S_{67} to S_{78}, and from S_{67} to S_{46}, respectively, with corresponding equivalent absolute values $|Y_{j,k}|$ $(t = t_P)$ of the time-integrated fluxes of electrons (k) through the boundaries A_j between these sectors, which quantify the arrows in the Lewis structure.

As second step, integration of the one-electron density in sectors $S_{ij}(G)$, where G denotes the geometric structures of either R or P, yields the total numbers $N_{ij,\mathrm{total}}(G)$ of all electrons in sectors $S_{ij}(G)$. They may be decomposed into the corresponding partial numbers $N_{ij,k}(G)$ of electrons in $S_{ij}(G)$, which occupy pericyclic (k = peri), other valence (k = oval), and core (k = core) electrons. These occupation numbers sum up to the numbers

$$N_{ij,\mathrm{val}}(G) = N_{ij,\mathrm{peri}}(G) + N_{ij,\mathrm{oval}}(G) \quad (16)$$

of all valence electrons, as well as to the total numbers

$$N_{ij,\mathrm{total}}(G) = N_{ij,\mathrm{val}}(G) + N_{ij,\mathrm{core}}(G) \quad (17)$$

of electrons in sectors $S_{ij}(G)$, analogous to eq 15 for the special cases $\xi = \xi_R$ $(G = R)$ and $\xi = \xi_P$ $(G = P)$.

The C_s symmetry implies that

$$N_{78,k}(G) = N_{23,k}(G) \quad (18)$$

$$N_{67,k}(G) = N_{34,k}(G) \quad (19)$$

and the $N_{ij,k}(P)$ values are equal to the equivalent $N_{i'j',k}(R)$, e.g., $N_{23,k}(P) = N_{34,k}(R)$. In order to predict the values of the net electron transfer from R to P, it suffices, therefore, to calculate the numbers of electrons in the sectors of the reactant, summing up to

$$N_k = N_{82,k}(R) + 2N_{23,k}(R) + 2N_{34,k}(R) + N_{46,k}(R) \quad (20)$$

Hence all the requested occupation numbers can be expressed in terms of just three numbers: $N_{82,k}(R)$, $N_{23,k}(R)$, and $N_{46,k}(R)$. The results for the numbers of electrons $N_{ij,k}(G)$ in sectors S_{ij} are listed in Table 1, for G = R and P.

As third step, the $N_{ij,k}(R)$ values are used to evaluate the net total and partial changes of the numbers of electrons, that is, the net accumulated fluxes into or out of the sectors S_{ij}:

$$Y_{ij,k} = N_{ij,k}(P) - N_{ij,k}(R) = Y_{i,k} - Y_{j,k} \quad (21)$$

(cf. eqs 7 and 14). Positive or negative values of $Y_{ij,k}$ indicate corresponding electron gains or losses, respectively. In particular,

$$Y_{82,k} = N_{82,k}(P) - N_{82,k}(R) = N_{46,k}(R) - N_{82,k}(R) = -Y_{46,k} \quad (22)$$

$$Y_{23,k} = N_{23,k}(P) - N_{23,k}(R) = N_{34,k}(R) - N_{23,k}(R) = -Y_{34,k} \quad (23)$$

for sectors S_{82}, S_{46} and S_{23}, S_{34}, respectively. The results are also listed in Table 1.

Table 1. Numbers of Electrons ($N_{ij,k}(G)$) in Pericyclic (k = peri), Other Valence (k = oval), All Valence (k = val), Core (k=core), and All (k = total) Orbitals, in the Sectors $S_{ij}(G)$ with Neighboring Carbon Atoms Ci and Cj of SBV, for the Geometric Structures G of the Reactants R and Products P (cf. Scheme 1, Figure 2, and eqs 21−23)[a]

	$N_{82,k}(R)$ $N_{46,k}(P)$	$N_{23,k}(R)$ $N_{78,k}(R)$ $N_{34,k}(P)$ $N_{67,k}(P)$	$N_{34,k}(R)$ $N_{67,k}(R)$ $N_{23,k}(P)$ $N_{78,k}(P)$	$N_{46,k}(R)$ $N_{82,k}(P)$	N_k	$Y_{82,k}$ $-Y_{46,k}$	$Y_{23,k}$ $Y_{78,k}$ $-Y_{34,k}$ $-Y_{67,k}$
peri	1.49	0.71	1.03	1.03	6	−0.46	0.32
oval	7.51	4.80	3.94	9.01	34	1.50	−0.86
val	9.00	5.51	4.97	10.04	40	1.04	−0.54
core	4.00	2.00	2.00	4.00	16	0.00	0.00
total	13.00	7.51	6.97	14.04	56	1.04	−0.54

[a] N_k is the sum of the $N_{ij,k}$ in all sectors S_{ij}. The $Y_{ij,k} = N_{ij,k}(P) - N_{ij,k}(R)$ values denote the corresponding changes of the numbers of electrons in sectors S_{ij}, from the reactants to the products. Positive and negative values correspond to gains or losses of electrons (k) in sectors S_{ij}.

dx.doi.org/10.1021/jp110365g |J. Phys. Chem. B 2011, 115, 5476–5483

Table 2. Numbers of Electrons ($Y_{j,k}$) in Pericyclic (k = peri), Other Valence (k = oval), All Valence (k = val), Core (k = core), and All (k = total) Orbitals, Which Are Transferred from Sector S_{ij} to the Neighboring One S_{jl} through the Boundary A_j, during the Cope Rearrangement of SBV[a]

	$Y_{2,k} = -Y_{8,k}$		$Y_{4,k} = -Y_{6,k}$		$Y_{7,k} = -Y_{3,k}$	
	cl[b]	QD[c]	cl[b]	QD[c]	cl[b]	QD[c]
peri	0.23	0.22	0.23	0.22	0.09	0.09
oval	−0.75	−0.74	−0.75	−0.75	−0.11	−0.08
val	−0.52	−0.52	−0.52	−0.53	−0.02	0.01
core	0.00	0.00	0.00	0.00	0.00	0.00
total	−0.52	−0.52	−0.52	−0.53	−0.02	0.01

[a] Small deviations of the net classical and quantum dynamics results are due to wavepacket dispersion (see Figure 1). The values for $Y_{j,\mathrm{peri}}$ are assigned to the pincer-motion-type set of curved arrows in the Lewis structure (see Figure 3). [b] Net classical results (eqs 24−26). [c] Net quantum dynamical results (eqs 27−29) for $t_P - t_R = t_r = 27.3$ fs.

As a fourth step, the time-integrated fluxes $Y_{j,k}$ of electrons (k), which have been transferred from bond Ci−Cj to Cj−Cl through the boundary A_j during the Cope rearrangement of SBV are calculated as

$$Y_{2,k} = -Y_{8,k} = -Y_{82,k}/2 \quad (24)$$

$$Y_{4,k} = -Y_{6,k} = Y_{46,k}/2 = -Y_{82,k}/2 \quad (25)$$

(cf. eqs 14 and 22). In order to determine the number $Y_{7,k}$ of electrons which are transferred from sector S_{67} to S_{78} through the boundary A_7, or equivalently from S_{34} to S_{23} through A_3, $Y_{3,k} = -Y_{7,k}$, we note that it contributes to the overall electron gain in sector S_{78}, or equivalently S_{23}. The other contribution is $Y_{2,k} = -Y_{8,k}$ (see eq 24). Hence

$$Y_{7,k} = Y_{78,k} + Y_{8,k} = -Y_{3,k} = Y_{23,k} - Y_{2,k}. \quad (26)$$

The results (eqs 24−26) are listed in Table 2 and summarized in Figure 3. The numbers of pericyclic electrons $Y_{j,k}$ (k = peri) that are transferred from S_{ij} to S_{jl} through A_j thus quantify the pincer-motion-type set of arrows in the Lewis structure. The transfer of electrons in other valence orbitals has significant contributions of the σ-like bonds of the CH groups, which move, for example, from the edge of the sector S_{82} toward its interior, that is, with direction opposite to the pericyclic electrons. As a consequence, the net electron transfer of all electrons is opposite to pericyclic electron transfer. This is irrevelant for the rearrangement of the electrons in the carbon chain, that is, subsequently, we focus on the pericyclic electrons.

Time-Dependent Analysis. Equations 16−26, Tables 1−2, Scheme 1, and Figures 2 and 3 are for the net results of electron numbers and time-integrated bond-to-bond fluxes from the reactant R to the product P in the classical limit. The corresponding quantum dynamical time evolution is obtained, in the framework of the BOA, in terms of the time-dependent nuclear wave function $\Psi_{nu}(\xi,t)$ ($t_R \le t \le t_P$) (eq 1) and density $\rho_{nu}(\xi,t) = |\Psi_{nu}(\xi,t)|^2$. The reactant is prepared as described in the nuclear quantum dynamics part of the Theory and Methods section.

The reaction time $t_r = t_P - t_R$ is the time that the center of the wavepacket takes to travel from ξ_R to ξ_P. In the present case, t_r = 27.3 fs. Figure 1 shows snapshots of the nuclear probability density at $t = t_R = 0$ fs, $t = t_B = 13.4$ fs, and $t = t_P = 27.3$ fs.

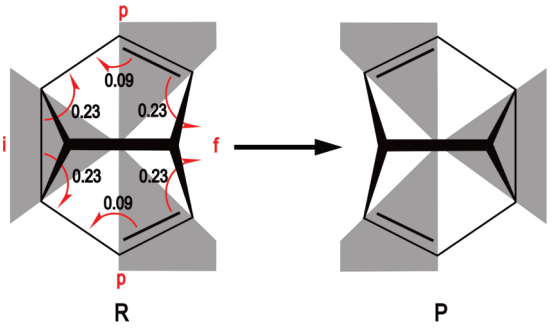

Figure 3. Quantification of the pincer-motion-type set of arrows in the Lewis structure of SBV. The numbers $|Y_{j,\mathrm{peri}}|$ specify the numbers of pericyclic electrons, which correspond to the rearranging electrons according to the Lewis structures. These are transferred from sector S_{ij} for bond Ci−Cj across the boundary A_j to the neighboring sector S_{jl} for bond Cj−Cl, in the direction of the arrow. They are evaluated by quantum simulations of the Cope rearrangement of SBV (see text and Table 2). The labels i, f, and p are for the initial (i) dominant fluxes out of the breaking bond C8−C2 (clockwise notation), for the final (f) dominant fluxes into the new bond C4−C6, and for the perpetual (p) rather small fluxes, which achieve double bond shifting.

The previous net results are recovered as classical limits of the quantum expression (eq 10) $\bar{N}_{ij,k}(t_R) \approx N_{ij,k}(R)$ and $\bar{N}_{ij,k}(t_P) \approx N_{ij,k}(P)$. Here and below, the approximate equality indicates small deviations of the net classical and quantum dynamical results, due to nuclear wavepacket dispersion, as shown in Figure 1.

By analogy with eqs 24−26, the time-integrated fluxes (see eq 11) of electrons due to transfer of electrons in orbitals k from Ci−Cj bond in sector S_{ij} to the neighboring Cj−Cl bond in sector S_{jl} through A_j are

$$\bar{Y}_{2,k}(t) = -\bar{Y}_{8,k}(t) = -\bar{Y}_{82,k}(t)/2 \quad (27)$$

$$\bar{Y}_{4,k}(t) = -\bar{Y}_{6,k}(t) = \bar{Y}_{46,k}(t)/2 \quad (28)$$

as well as

$$\bar{Y}_{7,k}(t) = -\bar{Y}_{3,k}(t) = \bar{Y}_{23,k}(t) - \bar{Y}_{2,k}(t) \quad (29)$$

The results (eqs 27−29) for the time evolution of the numbers of pericyclic electrons that are transferred between the neighboring bonds are illustrated in Figure 4A. In the limit $t \to t_P$, these quantum dynamical (QD) results approach the analogous net classical results (eqs 24−26; cf. Table 2). In particular, $\bar{Y}_{2,k}(t)$ and $\bar{Y}_{4,k}(t)$ form hystereses:

$$\bar{Y}_{2,k}(t) - \bar{Y}_{2,k}(t_R) \approx -\bar{Y}_{4,k}(t_R + t_P - t) + \bar{Y}_{4,k}(t_P) \quad (30)$$

For the ideal reference without any dispersion, the hystereses possess inversion centers at $(t_r/2 = (t_P - t_R)/2, (\bar{Y}_{4,k}(t_P) - \bar{Y}_{4,k}(t_R))/2)$. The time derivatives of the number of electrons in orbitals k, which have been transferred from the Ci−Cj bond to the neighboring Cj−Cl bond through the boundary A_j, are the corresponding fluxes

$$F_{j,k}(t) = \frac{d}{dt}\bar{Y}_{j,k}(t) \quad (31)$$

(cf. eq 13). These are documented in Figure 4B. The inversion symmetry of the hysteresis for the time-integrated fluxes implies corresponding symmetries of the fluxes,

$$F_{2,k}(t) \approx F_{4,k}(t_R + t_P - t) \quad (32)$$

The special results for k = peri may be interpreted as corresponding bond-to-bond fluxes of pericyclic electrons during

dx.doi.org/10.1021/jp110365g |J. Phys. Chem. B 2011, 115, 5476–5483

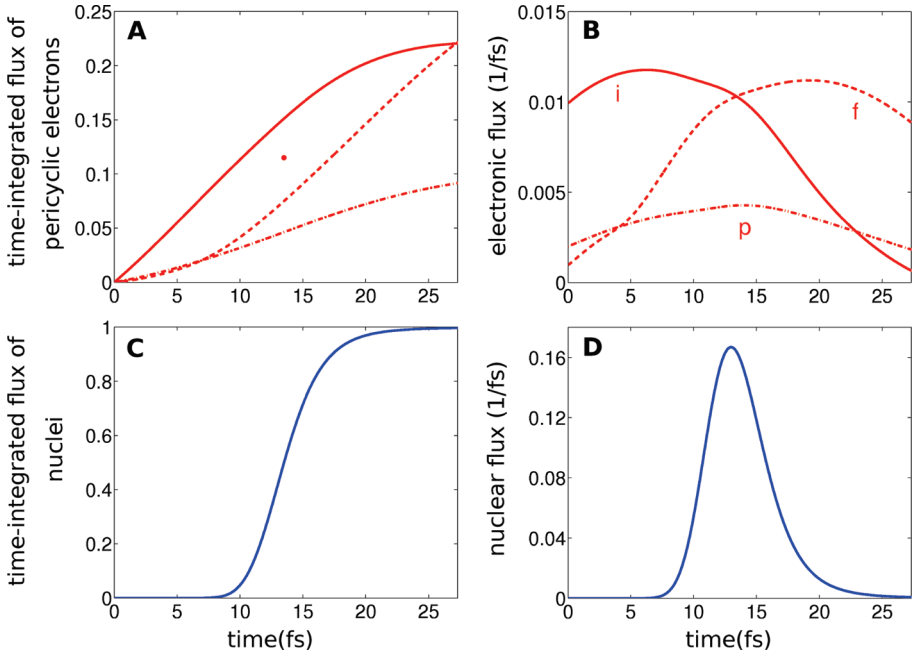

Figure 4. Time evolutions of the electronic (panels A and B) and nuclear (panels C and D, note the different scales) fluxes (B, D) and time-integrated fluxes (A, C) during Cope rearrangement of SBV, from $t = t_R = 0$ fs for the reactant R to $t = t_P = 27.3$ fs for the product P (cf. Figure 1). The reactants are prepared as described in the text. The results for the electrons are for the fluxes $F_{j,k}(t)$ and time-integrated fluxes $Y_{ij,k}(t)$ of the pericyclic electrons (k = peri). Continuous lines are for the initial (i) electron transfers from the carbon bond C8−C2 (clockwise notation) to the neighboring ones, C2−C3 or C7−C8. Dashed lines are for the final (f) electron transfers from bonds C3−C4 or C6−C7 to C4−C6. Dash-dotted lines are for the perpetual (p) electron transfers from C6−C7 to C7−C8 or equivalently from C3−C4 to C2−C3. (Compare with symbols i, f, and p in Figure 3.) The continuous and dashed lines for the time-integrated fluxes form a hysteresis with an inversion center, indicated by a dot (cf. eq 30).

Cope rearrangement of SBV, during 27.3 fs. The pattern of the fluxes is in accord with the pincer-motion-type set of arrows in the Lewis structure with C_s symmetry (see Figure 3).

The hysteresis-type time evolutions of the time-integrated electronic fluxes (Figure 4A) allow one to assign different arrows in the Lewis structures in Figure 3, which symbolize dominant initial (i) or final (f) bond-to-bond fluxes. In particular, $F_{2,k}(t) = -F_{8,k}(t)$ describe the dominant initial flux of pericyclic electrons (k = peri) out of the bond C8−C2, which is broken; subsequently, this flux slows down as t approaches t_P. In contrast, $F_{4,k}(t) = -F_{6,k}(t)$ display the opposite trend, that is, slow initial flux of pericyclic electrons into the new bond C4−C6, which speeds up and becomes the dominant final process for $t \rightarrow t_P$. For comparison, $F_{7,k}(t) = -F_{3,k}(t)$ values describe perpetual (p) rather small electronic fluxes, which account for the double bond shifting of SBV; the corresponding arrows are labeled (p) in Figure 3.

For comparison, we also show the corresponding fluxes $F_{nu}(t)$ as well as the time-integrated fluxes $Y_{nu}(t)$ of the nuclei C2, C4, C6, or C8, which pass through the nuclear observer planes (illustrated by green horizontal dashed lines in Figure 1) during the Cope rearrangement of SBV in Figure 4D and Figure 4C, respectively. They are evaluated as

$$Y_{nu}(t) = P_{nu}(\xi > 0, t) - P_{nu}(\xi > 0, t_R) \qquad (33)$$

where the population $P_{nu}(\xi > 0,t)$ denotes the integrated nuclear density $\rho_{nu}(\xi,t)$ in the domain of the products, $\xi > 0$. Again, the nuclear fluxes are evaluated as time derivatives of the corresponding time-integrated fluxes

$$F_{nu}(t) = \frac{d}{dt} Y_{nu}(t) \qquad (34)$$

As expected, the time-integrated nuclear fluxes at the end of the forward reaction are close to 1, meaning that the nuclei C2, C4, C6, and C8 pass through the observer planes essentially completely (cf. Figure 1). Moreover, the nuclear fluxes and time-integrated fluxes change rather quickly, compared to the overall smooth behavior of the smaller electronic fluxes and time-integrated fluxes, respectively. This difference is due to the different masses and the corresponding rather compact, localized nuclear wavepackets, compared to delocalized electronic ones.[18]

CONCLUSION

The present case study demonstrates that a well chosen set of curved arrows in Lewis structures may be equipped with additional meanings and quantitative information, beyond the traditional symbol for net electron transfers: They symbolize the directions of electronic bond-to-bond fluxes, and one may assign the numbers of electrons that are transferred from bond to bond, as well as labels for the time sequence, from electronic fluxes that dominate initially (i), to others that take over finally (f), due to hysteresis-type time evolutions of the time-integrated electronic fluxes (Figure 4A), or still others that flow perpetually (p). The present example (Figures 3 and 4) implies that during Cope rearrangement of SBV, pericyclic electrons start to flow first of all out of the breaking bond, whereas they enter the new bond only toward the end of the pericyclic reaction. This means asynchronous electronic fluxes during synchronous rearrangement of all the nuclei.

From the methodologic point of view, the present paper is an extension of ref 18, serving as a proof-of-principle that should stimulate investigations of the coupled electronic and nuclear fluxes during other pericyclic reactions. The predicted effects

should become observable by emerging techniques of femto- to attosecond time-resolved spectroscopy, including three-dimensional (3D) photoelectron imaging of ultrafast electronic-nuclear dynamics in aligned molecules,[34] high-harmonic interferometry as an effective approach to resolve multielectron dynamics with sub-angstrom spatial and even attosecond temporal resolutions,[33,36] femtosecond impulsive stimulated X-ray Raman scattering for observations of the time evolutions of all valence electronic states within the pulse bandwidths,[32] or electron diffraction techniques for four-dimensional (4D) imaging with free electrons[35] (for a recent review, see ref 79).

Following the advice of our colleague from Organic Chemistry, Prof. H. Quast (Würzburg University), we would like to conclude this paper with a take-home message: The curved arrows in Lewis structures contain sleeping beauty, i.e., they may not only symbolize the outcome of the pericyclic reaction that is expressed by the Lewis structure of the product, but also the electronic fluxes during the reaction. Firstly, there is a firm quantum mechanical basis for choosing the unique qualitative pattern of the set of curved arrows representing bond-to-bond electron transfers during pericyclic reactions, in the electronic ground state. In contrast with "pericyclic" patterns of clockwise or anticlockwise sets of curved arrows (which may be suggested by the term "pericyclic reactions", but which are actually associated with reactions in excited electronic states), the topology of the appropriate set of arrows tends to represent pincer-type motions of electrons during the reactions. Secondly, quantum quantification of the individual arrows yields rather small values for the numbers of electrons that are transferred from bond to bond (much below one electron per curved arrow) − this is a consequence of electron delocalization. For example, it is not at all necessary that the formation of a new bond is associated with the flux of two electrons out of the neighboring bond(s), because a significant fraction of those electrons occupies part of the nascent bond already before the reaction, due to delocalization. Thirdly, in addition to pericyclic electron fluxes, there are even stronger fluxes of other valence electrons in opposite direction. Fourthly, the individual bond-to-bond fluxes of electrons may have characteristic time evolutions that are not necessarily synchronous with the nuclear rearrangement. For example, in the present application to the Cope rearrangement of SBV, the nuclear motions associated with breaking the C8−C2 bond (cyclic notation; cf. Scheme 1) and the formation of the C4−C6 bond are synchronous, but the flux of the pericyclic electrons is asynchronous, that is, initially (i) they flow out of the breaking bond until finally (f) they enter the new bond (cf. Figure 2). Since the overall reaction takes only less than 30 fs, these subtle details are irrelevant for the total outcome of the reaction, but of course they are fascinating and also stimulating concerning the emerging experimental techniques for monitoring these processes in the femto-to-attosecond time domain.[79]

AUTHOR INFORMATION

Corresponding Author

*E-mail: bredt@chemie.fu-berlin.de (T.B.); jmanz@chemie.fu-berlin.de (J.M.).

Present Addresses

[||]Max-Born Institut, 12489 Berlin, Germany.

ACKNOWLEDGMENT

We would like to thank our colleagues from Organic Chemistry, Professors H. Ikeda (Osaka Prefecture University), D. Lenoir (Technische Universität München), H. Quast (Universität Würzburg), H.-U. Reissig, and C. Schalley (Freie Universität Berlin, FUB), for advice, and Dr. habil. A. Kenfack (FUB), A. Kaushik (IIT Bombay), and M. Berg (FUB) for exploratory model calculations, Professors D.J. Diestler (University of Nebraska-Lincoln) and H. Kono (Tohoku University, Sendai) and K. Takatsuka (Tokyo University) for stimulating discussions. Financial support from the Center for Scientific Simulations (FUB), Deutsche Forschungsgemeinschaft (DFG, project Ma 515/25-1), from the DFG research center MATHEON, and the Fonds der Chemischen Industrie is also gratefully acknowledged.

REFERENCES

(1) Desimoni, G.; Tacconi, G.; Barco, A.; Pollini, G. P. *Natural Products Synthesis through Pericyclic Reactions*; American Chemical Society: Washington, DC, 1987.
(2) Berson, J. A. In *Rearrangements in Ground and Excited States*; de Mayo, P., Ed.; Academic Press: New York, 1980; Vol. 1, p 311.
(3) Lowry, T. H.; Richardson, K. S. *Mechanism and Theory in Organic Chemistry*; Harper and Row: New York, 1987.
(4) Anslyn, E. V.; Dougherty, D. A. *Modern Physical Organic Chemistry*; University Science Books: Sausalito, CA, 2006.
(5) Smith, M. B.; March, J. *Advanced Organic Chemistry: Reactions, Mechanisms, and Structure*; Wiley: Hoboken, NJ, 2007.
(6) Vollhardt, K. P. C.; Schore, N. E. *Organic Chemistry − Structure and Function*; Freeman: New York, 2007.
(7) Wilkins, R. G. *Kinetics and Mechanism of Reactions of Transition Metal Complexes*; Verlag Chemie: Weinheim, Germany, 1991.
(8) Jordan, R. B. *Reaction Mechanisms of Inorganic and Organometallic Systems*; Oxford University Press: Oxford, U.K., 2007.
(9) Mathews, C. K.; van Holde, K. E.; Ahern, K. G. *Biochemistry*; Prentice Hall: Upper Saddle River, NJ, 1999.
(10) Nelson, D. L.; Cox, M. M. *Lehninger Principles of Biochemistry*; Freeman: New York, 2009.
(11) Woodward, R. B.; Hoffmann, R. *The Conservation of Orbital Symmetry*; Verlag Chemie: Weinheim, Germany, 1970.
(12) Houk, K. N.; Li, Y.; Evanseck, J. D. *Angew. Chem., Int. Ed.* **1992,** *31*, 682.
(13) Wiest, O.; Montiel, D. C.; Houk, K. N. *J. Phys. Chem. A* **1997,** *101*, 8378.
(14) Carpenter, B. K. *Angew. Chem., Int. Ed.* **1998,** *37*, 3340.
(15) Dewar, M. J. S. *J. Am. Chem. Soc.* **1984,** *106*, 209.
(16) Borden, W. T.; Loncharich, R. J.; Houk, K. N. *Annu. Rev. Phys. Chem.* **1988,** *39*, 213.
(17) Xu, L.; Doubleday, C. E.; Houk, K. N. *J. Am. Chem. Soc.* **2010,** *132*, 3029.
(18) Barth, I.; Hege, H. C.; Ikeda, H.; Kenfack, A.; Koppitz, M.; Manz, J.; Marquardt, F.; Paramonov, G. K. *Chem. Phys. Lett.* **2009,** *481*, 118.
(19) Miller, W. H. *J. Chem. Phys.* **1974,** *61*, 1823.
(20) Miller, W. H. *Acc. Chem. Res.* **1993,** *26*, 174.
(21) Miller, W. H. *J. Phys. Chem. A* **1998,** *102*, 793.
(22) Manthe, U.; Seideman, T.; Miller, W. H. *J. Chem. Phys.* **1994,** *101*, 4759.
(23) Henriksen, N. E.; Hansen, F. Y. *Theories of Molecular Reaction Dynamics*; Oxford University Press, Inc.: New York, 2008; Chapter 4, p 89.
(24) Kenfack, A.; Marquardt, F.; Paramonov, G. K.; Barth, I.; Lasser, C.; Paulus, B. *Phys. Rev. A* **2010,** *81*, 052502.
(25) von den Hoff, P.; Znakovskaya, I.; Zherebtsov, S.; Kling, M. F.; de Vivie-Riedle, R. *Appl. Phys. B: Laser Opt.* **2010,** *98*, 659.
(26) Okuyama, M.; Takatsuka, K. *Chem. Phys. Lett.* **2009,** *476*, 109.
(27) Yonehara, T.; Takatsuka, K. *Chem. Phys.* **2009,** *366*, 115.
(28) Nagashima, K.; Takatsuka, K. *J. Phys. Chem. A* **2009,** *113*, 15240.

(29) Niikura, H.; Villeneuve, D. M.; Corkum, P. B. *Phys. Rev. Lett.* **2005,** *94*, 083003.
(30) Chelkowski, S.; Yudin, G. L.; Bandrauk, A. D. *J. Phys. B* **2006,** *39*, S409.
(31) Goulielmakis, E.; Loh, Z.-H.; Wirth, A.; Santra, R.; Rohringer, N.; Yakovlev, V. S.; Zherebtsov, S.; Pfeifer, T.; Azzeer, A. M.; Kling, M. F.; Leone, S. R.; Krausz, F. *Nature* **2010,** *466*, 739.
(32) Mukamel, S.; Abramavicius, D.; Yang, L.; Zhuang, W.; Schweigert, I. V.; Voronine, D. V. *Acc. Chem. Res.* **2009,** *42*, 553.
(33) Smirnova, O.; Mairesse, Y.; Patchkovskii, S.; Dudovich, N.; Villeneuve, D.; Corkum, P.; Ivanov, M. Y. *Nature* **2009,** *460*, 972.
(34) Bisgaard, C. Z.; Clarkin, O. J.; Wu, G.; Lee, A. M. D.; Gessner, O.; Hayden, C. C.; Stolow, A. *Science* **2009,** *323*, 1464.
(35) Baum, P.; Zewail, A. H. *Chem. Phys.* **2009,** *366*, 2.
(36) Wörner, H. J.; Bertrand, J. B.; Kartashov, D. V.; Corkum, P. B.; Villeneuve, D. M. *Nature* **2010,** *466*, 604.
(37) Cope, A. C.; Hardy, E. M. *J. Am. Chem. Soc.* **1940,** *62*, 441.
(38) Zimmerman, H. E.; Grunewald, G. L. *J. Am. Chem. Soc.* **1966,** *88*, 183.
(39) Cheng, A. K.; Anet, F. A. L.; Mioduski, J.; Meinwald, J. *J. Am. Chem. Soc.* **1974,** *96*, 2887.
(40) Martin, H.-D.; Urbanek, T. *J. Am. Chem. Soc.* **1985,** *107*, 5532.
(41) Bergmann, K.; Görtler, S.; Manz, J.; Quast, H. *J. Am. Chem. Soc.* **1993,** *115*, 1490.
(42) Quast, H.; Herkert, T.; Witzel, A.; Peters, E. M.; Peters, K.; von Schnering, H. G. *Chem. Ber.* **1994,** *127*, 921.
(43) Williams, R. V.; Kurtz, H. A. *J. Chem. Soc., Perkin Trans. 2* **1994,** *2*, 147.
(44) Dohle, M.; Manz, J.; Paramonov, G. K. *Ber. Bunsen-Ges. Phys. Chem.* **1995,** *99*, 478.
(45) Dohle, M.; Manz, J.; Paramonov, G. K.; Quast, H. *Chem. Phys.* **1995,** *197*, 91.
(46) Korolkov, M. V.; Manz, J.; Paramonov, G. K. *J. Chem. Phys.* **1996,** *105*, 10874.
(47) Jiao, H.; Nagelkerke, R.; Kurtz, H. A.; Williams, R. V.; Borden, W. T.; von Ragué Schleyer, P. *J. Am. Chem. Soc.* **1997,** *119*, 5921.
(48) Jackman, L. M.; Fernandes, E.; Heubes, M.; Quast, H. *Eur. J. Org. Chem.* **1998,** 2209.
(49) Quast, H.; Seefelder, M. *Angew. Chem., Int. Ed.* **1999,** *38*, 1064.
(50) Williams, R. V. *Eur. J. Org. Chem.* **2001,** 227.
(51) Williams, R. V. *Chem. Rev.* **2001,** *101*, 1185.
(52) Staroverov, V. N.; Davidson, E. R. *J. Mol. Struct.* **2001,** *573*, 81.
(53) Goren, A. C.; Hrovat, D. A.; Seefelder, M.; Quast, H.; Borden, W. T. *J. Am. Chem. Soc.* **2002,** *124*, 3469.
(54) Garavelli, M.; Bernardi, F.; Cembran, A.; Castaño, O.; Frutos, L. M.; Merchán, M.; Olivucci, M. *J. Am. Chem. Soc.* **2002,** *124*, 13770.
(55) Brown, E. C.; Henze, D. K.; Borden, W. T. *J. Am. Chem. Soc.* **2002,** *124*, 14977.
(56) Seefelder, M.; Heubes, M.; Quast, H.; Edwards, W. D.; Armantrout, J. R.; Williams, R. V.; Cramer, C. J.; Goren, A. C.; Hrovat, D. A.; Borden, W. T. *J. Org. Chem.* **2005,** *70*, 3437.
(57) Shaik, S. S.; Hiberty, P. C. *A Chemist's Guide to Valence Bond Theory*; Wiley: Hoboken, NJ, 2008.
(58) Williams, R. V. In *Strained Hydrocarbons*; Dodziuk, H., Ed.; Wiley: Weinheim, Germany, 2009; pp 399−424.
(59) Brown, E. C.; Bader, R. F. W.; Werstiuk, N. H. *J. Phys. Chem. A* **2009,** *113*, 5254.
(60) Greve, D. R. *J. Phys. Org. Chem.* [Online early access]. DOI: 10.1002/poc.1731. Published Online: Jun 21, 2010.
(61) Rozgonyi, T.; Bartók-Pártay, A.; Stirling, A. *J. Phys. Chem. A* **2010,** *114*, 1207.
(62) Zhang, X.; Hrovat, D. A.; Borden, W. T. *Org. Lett.* **2010,** *12*, 2798.
(63) Born, M.; Oppenheimer, R. *Ann. Phys.* **1927,** *84*, 457.
(64) Born, M. *Nachr. Akad. Wiss. Göttingen, Math.-Phys. Kl., 2A: Math.-Phys.-Chem. Abt.* **1951,** *6*, 1.
(65) Born, M.; Huang, K. *Dynamical Theory of Chrystal Lattices*; Oxford University Press: London, 1954; Appendix VIII, pp 406−407.
(66) Iwakura, I.; Yabushita, A.; Kobayashi, T. *Chem. Lett.* **2010,** *39*, 374.
(67) Schwebel, A.; Brestel, M.; Yogev, A. *Chem. Phys. Lett.* **1984,** *107*, 579.
(68) Li, W.; Zhou, X.; Lock, R.; Patchkovskii, S.; Stolow, A.; Kapteyn, H. C.; Murnane, M. M. *Science* **2008,** *322*, 1207.
(69) Werner, H.-J.; Knowles, P. J.; Manby, F. R.; Schütz, M.; Celani, P.; Knizia, G.; Korona, T.; Lindh, R.; Mitrushenkov, A.; Rauhut, G.; Adler, T. B.; Amos, R. D.; Bernhardsson, A.; Berning, A.; Cooper, D. L.; Deegan, M. J. O.; Dobbyn, A. J.; Eckert, F.; Goll, E.; Hampel, C.; Hesselmann, A.; Hetzer, G.; Hrenar, T.; Jansen, G.; Köppl, C.; Liu, Y.; Lloyd, A. W.; Mata, R. A.; May, A. J.; McNicholas, S. J.; Meyer, W.; Mura, M. E.; Nicklass, A.; Palmieri, P.; Pflüger, K.; Pitzer, R.; Reiher, M.; Shiozaki, T.; Stoll, H.; Stone, A. J.; Tarroni, R.; Thorsteinsson, T.; Wang, M.; Wolf, A.; *MOLPRO*, version 2006.1, a package of ab initio programs; see http://www.molpro.net.
(70) Becke, A. D. *J. Chem. Phys.* **1993,** *98*, 5648.
(71) Lee, C.; Yang, W.; Parr, R. G. *Phys. Rev. B* **1998,** *37*, 785.
(72) Dunning, T. H. *J. Chem. Phys.* **1989,** *90*, 1007.
(73) Schmidt, B.; Lorenz, U. *WavePacket* (version 4.7), a program package for quantum mechanical wavepacket propagation and time-dependent spectroscopy; see http://wavepacket.sourceforge.net (Freie Universität: Berlin, 2009).
(74) Stalling, D.; Westerhoff, M.; Hege, H. C. In *The Visualization Handbook*; Hansen, C. D., Johnson, C. R., Eds.; Elsevier: Amsterdam, 2005; Chapter 38, pp 749−767.
(75) Pipek, J.; Mezey, P. G. *J. Chem. Phys.* **1989,** *90*, 4916.
(76) Barth, I.; Manz, J.; Shigeta, Y.; Yagi, K. *J. Am. Chem. Soc.* **2006,** *128*, 7043.
(77) Kanno, M.; Kono, H.; Fujimura, Y. *Angew. Chem., Int. Ed.* **2006,** *45*, 7995.
(78) Kanno, M.; Kono, H.; Fujimura, Y.; Lin, S. H. *Phys. Rev. Lett.* **2010,** *104*, 108302.
(79) Krausz, F.; Ivanov, M. *Rev. Mod. Phys.* **2009,** *81*, 163.